Title

Particulate Cadmium Accumulation in the Mesopelagic Ocean.

Journal

Global Biogeochemical Cycles, 39(1)

ISSN

0886-6236

Authors

Laubach, Allison

Lee, J-M

Sieber, M

et al.

Publication Date

2025

DOI

10.1029/2024GB008281

Peer reviewed

Global Biogeochemical Cycles

RESEARCH ARTICLE
10.1029/2024GB008281

Special Collection:
The U.S. GEOTRACES Pacific Meridional Transect (GP15)

Particulate Cadmium Accumulation in the Mesopelagic Ocean

A. Laubach[1], J.-M. Lee[1], M. Sieber[2], N. T. Lanning[3,4], J. N. Fitzsimmons[3], T. M. Conway[2], and P. J. Lam[1]

[1]Department of Ocean Sciences, University of California Santa Cruz, Santa Cruz, CA, USA, [2]College of Marine Science, University of South Florida, St. Petersburg, FL, USA, [3]Department of Oceanography, Texas A&M University, College Station, TX, USA, [4]Department of Earth, Atmospheric, & Planetary Science, Massachusetts Institute of Technology, Cambridge, MA, USA

Abstract Observations of dissolved cadmium (dCd) and phosphate (PO_4) suggest an unexplained loss of dCd to the particulate phase in tropical oxyclines. Here, we compile existing observations of particulate Cd and phosphorus (P), and present new data from the US GEOTRACES GP15 Pacific Meridional Transect to examine this phenomenon from a particulate Cd perspective. We use a simple algorithm to reproduce station depth profiles of particulate Cd and P via regeneration and possible subsurface accumulation. Our examination of regeneration reveals decoupling of particulate Cd and P driven by variable partitioning between two particulate pools with differing labilities. Further, we identify evidence for subsurface particulate Cd accumulation at 31 stations. Subsurface particulate Cd accumulation occurs most consistently in the mesopelagic tropical Pacific but can be found in all examined ocean basins. This accumulation is not well-correlated with dissolved oxygen or particulate sulfide concentration. Instead, we observe that particulate Cd accumulation occurs in regions where the concentration of dCd is relatively high compared to dissolved zinc (dZn) and speculate that it is the result of enhanced dCd biological uptake in response to the subsurface micronutrient balance.

Key Points:

- Vertical profiles show evidence of subsurface particulate Cd accumulation in the Equatorial Pacific and other ocean basins
- Variable regeneration of particulate Cd and P is driven by differences in partitioning into a refractory particulate pool
- Particulate Cd accumulation may be linked to subsurface trace metal micronutrient balance

Supporting Information:

Supporting Information may be found in the online version of this article.

Correspondence to:

A. Laubach,
alaubach@ucsc.edu

Citation:

Laubach, A., Lee, J.-M., Sieber, M., Lanning, N. T., Fitzsimmons, J. N., Conway, T. M., & Lam, P. J. (2025). Particulate cadmium accumulation in the Mesopelagic Ocean. *Global Biogeochemical Cycles*, *39*, e2024GB008281. https://doi.org/10.1029/2024GB008281

Received 30 JUN 2024
Accepted 13 DEC 2024

1. Introduction

Early observations of the trace metal cadmium (Cd) noted its vertical nutrient-like distribution and strong correlation with the macronutrient phosphate (PO_4) (Boyle et al., 1976; Bruland et al., 1978; de Baar et al., 1994). In the years since, expanded observation efforts have made it clear that dissolved Cd (dCd) has a dominantly nutrient-like distribution throughout the global oceans (Baars et al., 2014; Conway & John, 2015; Conway & Middag, 2024; Gerringa et al., 2021; John et al., 2018; Sieber et al., 2023b; Xie et al., 2015), including in margin regions with potentially complicated trace metal dynamics (Gutierrez-Mejia et al., 2016; Hernández-Candelario et al., 2019; Seo et al., 2022; Tian et al., 2023; Wong et al., 2021;). The one exception to this nutrient-like characterization is in the Arctic Ocean, where mixing dominates the dCd distribution (Zhang et al., 2019).

Overall, the nutrient-like distribution of dCd suggests that, like PO_4, Cd cycling is driven primarily by biological uptake in the surface and regeneration at depth, despite the non-essential physiological role of Cd in the biochemical machinery of phytoplankton cells (Lee & Morel, 1995) and Cd's observed toxicity to phytoplankton (Brand et al., 1986; Sunda & Huntsman, 1996; Tortell & Price, 1996). Precise Cd uptake mechanics remain unclear, with some work suggesting that Cd is passively transported through cellular membranes when mistaken for a more essential divalent metal (Horner et al., 2013). However, despite Cd's apparent toxicity, Cd can be used to alleviate zinc (Zn) stress in some phytoplankton (Cox & Saito, 2013; Lee & Morel, 1995; Xu et al., 2007) and specifically as a substitute in carbonic anhydrase by some diatoms (Lane & Morel, 2000). In fact, Cd uptake is enhanced when surface dCd concentrations are high (Horner et al., 2013) and when dissolved concentrations of other bioessential divalent metals such as iron (Fe) and manganese (Mn) are low (Cullen et al., 2003; Sunda & Huntsman, 2000). The multifactorial influences on Cd uptake yield a wide range of cellular quotas of Cd relative to phosphorus (P) across phytoplankton groups in different regions (Ho et al., 2003; Twining & Baines, 2013). Consequently, the observed ratio of total particulate Cd to P (Cd:P) in the euphotic zone and exported particles also varies widely (Black et al., 2019; Bourne et al., 2018; Roshan & DeVries, 2021).

Global dCd and PO_4 data compilations have been fit with a pseudo-linear correlation, recording a dCd:PO_4 ratio of ∼0.4 mmol:mol and a notable decrease in slope, or "kink," at PO_4 concentrations below ∼1.3 μM, although global compilations in the GEOTRACES era show more regional scatter (Conway & Middag, 2024; de Baar

et al., 1994). This "kink" has been explained by the influence of intermediate waters that have unique preformed dCd:PO_4 ratios due to biological metal uptake in the surface ocean regions where they form (Frew & Hunter, 1992). Variations in uptake stoichiometry, regeneration extent, and water mass mixing account for most dCd:PO_4 observations (Chen et al., 2024; Middag et al., 2018; Quay et al., 2015; Roshan & Wu, 2015; Sieber et al., 2023b).

However, despite our increasing understanding of dCd cycling, these processes do not fully describe some regional patterns in dCd:PO_4. Notably, decoupling of dCd from PO_4 has been described for several low-oxygen regions of the ocean (Conway & John, 2015; Guinoiseau et al., 2018; Janssen et al., 2014), attributed to loss of Cd from the dissolved phase relative to PO_4. Hypotheses for the decoupling of dCd from PO_4 in these regions include loss of dCd to the particulate phase via Cd sulfide (CdS) precipitation in low oxygen conditions (Janssen et al., 2014), Cd uptake by subsurface heterotrophs (Ohnemus et al., 2017), and variable regeneration rates for particulate Cd and P (Bourne et al., 2018). However, more recently, it has been shown that dissolved and particulate sulfides present under low-oxygen conditions of the Pacific Ocean are too low in concentration to support observed deficits in dCd (Buckley et al., 2024). Additionally, other work has shown that many of the observed deficits in dCd in the Atlantic and Pacific can alternatively be explained by a combination of variable stoichiometry of Cd:PO_4 during uptake alongside water mass mixing (de Souza et al., 2022). However, dCd:PO_4 observations below the expected linear trend in tropical oxyclines remain unexplained (de Souza et al., 2022). In the tropical South Pacific, where observations do suggest a removal of dCd relative to PO_4, a shoaled oxycline and fluorescence maxima combine to generate an environment where sulfide is produced by both assimilatory and dissimilatory processes, hypothesized to facilitate dCd loss to particles such as CdS (Buckley et al., 2024).

Crucially, however, variable regeneration, CdS precipitation, and heterotrophic uptake explanations all require consideration of dissolved-particulate partitioning of Cd relative to P, with previous studies often focusing only on the dissolved phase. It is thus beneficial to investigate and assess these hypotheses from the particulate perspective as well (de Souza et al., 2022). Here, we explore the effects of regeneration and subsurface particulate Cd accumulation on particulate Cd:P profiles. We present new data from the GEOTRACES GP15 Pacific Meridional Transect and compile existing international GEOTRACES particulate Cd and P observations from large volume pumps and bottle filtration (GEOTRACES Intermediate Data Product Group, 2023). We then discuss Cd:P patterns and consider the variable regeneration, CdS, and heterotroph hypotheses in the context of the particulate data and tropical oxycline dCd:PO_4 observations.

2. Methods

2.1. GP15 Sample Collection

The U.S. GEOTRACES GP15 Pacific Meridional Transect sampled from the Alaskan margin (56°N) to Tahiti (20°S) along the 152°W meridian. For a description of water mass distributions across the transect and their influence on dCd, see Sieber et al. (2023b). Size-fractionated particulate samples were collected at 23 full-depth stations (Figure 1) via dual flow path and large volume in situ pump filtration following standard GEOTRACES sampling procedures (Lam et al., 2018; Xiang & Lam, 2020). For this study, samples analyzed were collected on 142 mm diameter filter holders outfitted with a 51 μm polyester mesh prefilter (Sefar; large size fraction) followed by paired 0.8 μm polyethersulfone filters (Supor; small size fraction). We focus our analysis here on the 0.8–51 μm small size fraction, which accounts for nearly 90% of Cd and P concentrations over the depths of interest.

2.2. GP15 Particulate Cd and P Analysis

Supor filter particles were digested using a modified refluxing method (Ohnemus et al., 2014). Modifications are described by Xiang and Lam (2020) and summarized here. Briefly, a 1/16 slice of each filter was adhered to the wall of a pre-cleaned 15 mL Teflon vial to prevent submersion. Then, 2 mL of ultrapure 50% HNO_3/10% HF (v/v) digestion solution was added and allowed to reflux for 4 hr at 110°C. The cooled digestion solution was transferred to secondary vials and dried, then heated in ultrapure 50% HNO_3/15% H_2O_2 (v/v) and dried again. Finally, the samples were redissolved in ultrapure 5% HNO_3 and analyzed using Inductively Coupled Plasma Mass Spectrometry (Element XR, Thermo Scientific) at the UCSC Plasma Analytical Facility. Approximately 15 mg of certified reference materials BCR-414 (freshwater plankton) and PACS-2 (marine sediment) were digested and analyzed alongside samples. Blanks, detection limits, and reference material recoveries are shown in Table S1 in Supporting Information S1.

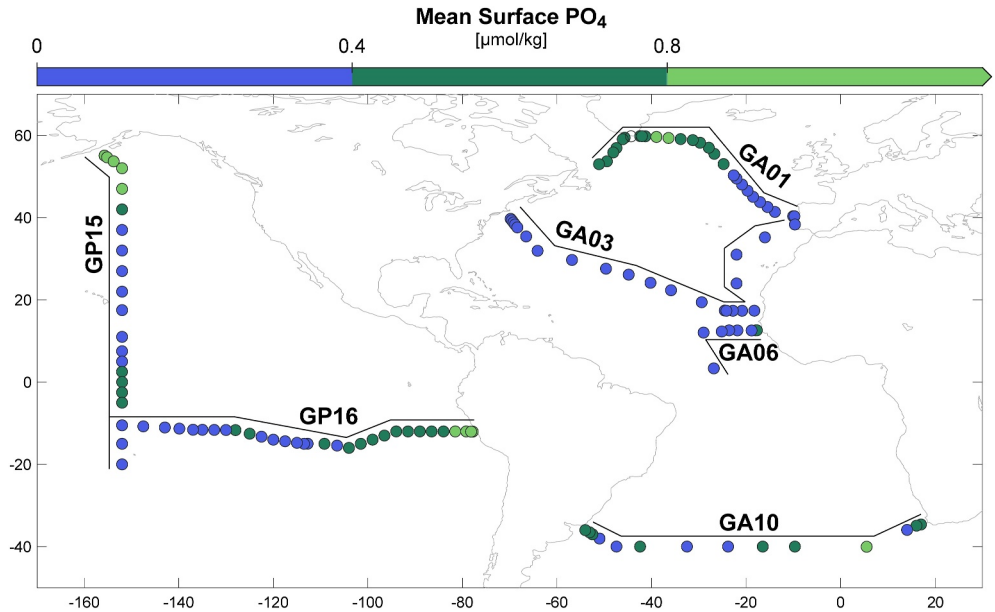

Figure 1. GEOTRACES stations with both particulate Cd and particulate P data were compiled for investigation in this study. Station colors correspond to the surface phosphate concentration regime based on World Ocean Atlas 2023 data (Garcia et al., 2024).

2.3. Additional Data Compilation

2.3.1. GP15 Dissolved Cd and Zn Data

Dissolved Cd and dZn data for GP15 were compiled from Sieber et al. (2023a), and Sieber et al., 2019; see those papers for details of sample collection, sample processing, analytical methods, and data quality.

2.3.2. Other Particulate and Dissolved Cd and P

Additional dCd and PO_4 data were retrieved from the GEOTRACES 2021 Intermediate Data Product (IDP; GEOTRACES Intermediate Data Product Group, 2023). Data from particles collected via in situ pumps as described above are referred to as pump data and were compiled for GEOTRACES cruises GP16 (Lee et al., 2018) and GA03 (Ohnemus & Lam, 2015). Data from particles collected via trace metal clean Go-Flo bottles are referred to as bottle data and were available from cruises GP16 (Figure S1 in Supporting Information S1; Ohnemus et al., 2017), GA01 (Gourain et al., 2019; Lemaitre et al., 2020), GA03 (Lam et al., 2015), GA06 (Bridgestock et al., 2018), and GA10 (Figure 1; Chen et al., 2024). Bottle particles were collected on 0.45 µm Supor filters. Because of the higher sampling resolution, bottle data was used for our analysis instead of pump data for GP16 (See Section 3.2 for discussion of bottle-pump differences). In contrast, we used pump data for GA03 because bottle data from that transect were limited to the upper water column. Dissolved trace metal data were obtained from the GEOTRACES IDP for cruises GP16 (John et al., 2018), GA01 (Tonnard et al., 2020), GA03 (Conway & John, 2015), and GA10 (Chen et al., 2024; GEOTRACES Intermediate Data Product Group, 2023). Additional information about the compiled data and cruise contexts can be found in their respective references.

2.3.3. Hydrographic Data

Because chlorophyll fluorescence and photosynthetically available radiation were not measured for all cruises, the euphotic zone depth (1% surface irradiance) was calculated using satellite-derived diffuse attenuation coefficients (MODIS-Aqua 8-day average, 4 km resolution; NASA Goddard Space Flight Center, 2018) encompassing the sampling date at each station:

$$z_{eu} = \frac{\ln(0.01)}{-K_D} \quad (1)$$

where z_{eu} is the euphotic zone depth and K_D is the diffuse attenuation coefficient at 490 nm (Figure S2 in Supporting Information S1). Other hydrographic data, including dissolved oxygen and PO_4, were retrieved from the GEOTRACES IDP (GEOTRACES Intermediate Data Product Group, 2023).

Each station was assigned to one of three surface nutrient regimes based on the World Ocean Atlas annual mean surface PO_4 concentrations (Figure 1; Garcia et al., 2024): Low (<0.4 μmol kg^{-1}), moderate (0.4–0.8 μmol kg^{-1}), and high (>0.8 μmol kg^{-1}). These ranges were chosen based on the median value in the data set (0.404 μmol kg^{-1}) such that the low nutrient regime stations have PO_4 concentrations below the global median and the high nutrient regime stations have PO_4 concentrations more than twice the global median.

2.4. Regeneration

We describe particulate Cd and P regeneration using a double exponential decay function fit to station data profiles. Exponential decay functions were chosen because they fit observations of decreasing particulate metal concentrations as a function of depth. Double exponential decay functions were utilized to directly describe and compare how the concentrations of different "forms" of particulate Cd and P are represented within the total concentration. Thus, we fit the data with a double exponential decay function on top of a constant background in each profile, as

$$C_z = C_{0,lab}\, e^{k_{lab} \cdot z} + C_{0,ref}\, e^{k_{ref} \cdot z} + C_{const} \quad (2)$$

where C_z is the concentration at depth z, C_0 is the initial concentration at the base of the euphotic zone, k is the decay constant in m^{-1}, z is depth below the euphotic zone, and C_{const} is the minimum concentration at that station determined from the data. The "lab" subscript denotes a more labile form of Cd or P, the "ref" subscript denotes a more refractory form, and the constant form is considered inert on the timescale of particles sinking to the seafloor. The parameters $C_{0,lab}$, $C_{0,ref}$, k_{lab}, and k_{ref} were fit such that C_z best matched the measured data. The parameter fits were constrained to be sensible: $C_{0,lab}$ and $C_{0,ref}$ had to be positive and not exceed the highest concentration measured at that station, and k_{lab} and k_{ref} had to be negative and not below −0.5 (see Section S1 in Supporting Information S1 for additional discussion). An example of the double exponential fits to particulate Cd and P as well as the resulting ratio of the fits is shown in Figure 2a.

The regeneration length scale for a pool was calculated as the inverse of its k value:

$$L = \left|\frac{1}{k}\right| \quad (3)$$

and has units of m. This length scale is the e-folding depth and therefore represents the depth below the euphotic zone at which approximately 63% of the initial particulate concentration has been removed by regeneration.

2.5. Accumulation

One of the goals of our study was to identify sites where a surplus of particulate Cd was observed compared with particulate P. Thus, we define "excess Cd" as when the particulate Cd concentration at a specific depth is higher than would be expected based on regeneration alone, and "Cd accumulation" as excess Cd at stations where there is not also excess P. This rationale assumes that particulate Cd profiles are one-dimensional, are dominated by gravitational sinking and regeneration processes, and are not affected by lateral mixing processes, primary production, or active transport such as by zooplankton diel vertical migration. To respect these assumptions, we used particulate P as a filter for non-Cd-specific processes and confined our analysis to depths between the base of the euphotic zone and 2,000 m for all stations except those from GP16. For GP16, analysis was limited to the upper 1,800 m to avoid the potential influence of a known hydrothermal plume from the southern East Pacific Rise (Fitzsimmons et al., 2017; Resing et al., 2015), which may act to add or remove trace elements to ocean waters, decoupling trace elements from macronutrient concentrations (Fitzsimmons & Steffen, 2024).

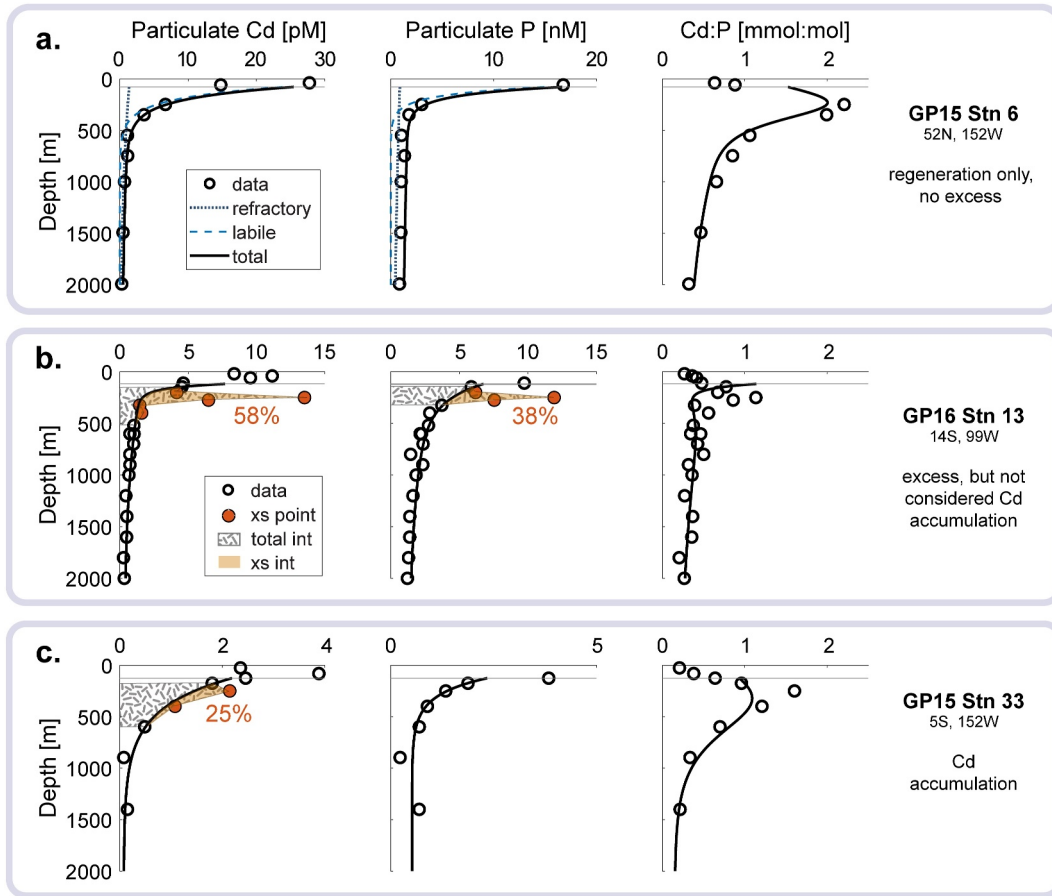

Figure 2. Example vertical particle profiles depicting three different regeneration fit scenarios. (a) Particulate Cd (left), P (center), and Cd:P (right) profiles from GP15 station 6. The dotted lines show the refractory pool portion of the regeneration fit equation (Equation 2 *ref*), dashed lines show the labile pool portion (Equation 2 *lab*), and black solid lines show the overall fit. There are no excess points at this station, so the original regeneration fits are shown. (b) Particulate Cd (left), P (center), and Cd:P (right) profiles from GP16 station 13. The orange circles show excess points that were removed before refitting the regeneration equations. The solid black line shows the overall fit (refractory and labile pool lines not shown for clarity). The hatched areas are the total integrated Cd or P over the depth of excess incidence. The shaded orange regions are the integrated excess. The orange number shows the percentage of the total integrated area attributed to excess. Because the excess percentage of P is greater than 20%, this station is not considered to have Cd-specific accumulation. (c) Particulate Cd (left), P (center), and Cd:P (right) profiles from GP15 station 33 showing Cd accumulation. Figure elements are as described in panel (b).

Profiles where regeneration fits were able to describe a large majority of the variation in observed particulate Cd:P ($R^2 \geq 0.90$) were excluded from the accumulation analysis, as their concentrations were understood to be explained by regeneration alone (Figure 2a). For the remaining profiles, which presumably include some particulate Cd excess, we aimed to identify the depths where the particulate Cd excess occurred and then calculate the excess compared to what was expected based on regeneration alone. To do this, we first used a systematic depth-by-depth data removal process to identify which depths hosted excess particulate Cd concentrations, removed those data points temporarily, and then used the remaining data for that profile to refit the regeneration-only curve for that station. This data removal and refit process involved assigning the first particulate Cd observation below the euphotic zone as an anchor point; therefore, it was not removed. Then, systematically, the first data point below the anchor point was removed from the data set and the regeneration equation refitted to the remaining data and fit statistics recorded. Then, the next deeper point was removed, and the regeneration equation (Equation 2) refit to the remaining data and fit statistics recorded. This process was repeated for all possible single-point removals and refits of points below the anchor point. Then, this systematic process was repeated again with a rolling removal of two consecutive data points with refits to the remaining data, then three consecutive data points

with refits to the remaining data. The equation fit requires a minimum of four remaining points; therefore, the maximum number of points removed varied by data availability for each profile up to a maximum of five.

Then, after all regeneration refits for a profile were completed and statistics gathered, we selected the fit for which the root-mean square error (RMSE) of the remaining data refit was the smallest. We refer to this chosen refit as "apparent regeneration." Finally, the removed data points were considered to be host excess particulate Cd if they had higher concentrations than the apparent regeneration concentration at the same depth.

Subsurface Cd accumulation is differentiated from excess particulate Cd by controlling for non-Cd-specific processes. To quantify subsurface Cd accumulation, we first integrated the excess particulate Cd over its depth range of incidence and compared it to the integrated particulate Cd of the apparent regeneration curve over the same depths. The excess points were linearly interpolated, and the depth range of incidence included the identified excess points and the nearest adjacent non-excess points. For example, for a profile with measurements every 100 m and excess points identified at 300 and 400 m, the range of incidence for the integration would be 200–500 m. We express accumulation as a fraction of the total integrated Cd (Cd_{xsfrac}, unitless) over the range of incidence. We then assumed that excesses in particulate P beyond regeneration, calculated in the same way as above but for P, could be used to diagnose non-Cd-specific excess processes that may present as accumulation, such as lateral particle transport, diel vertical migration, or other processes that could lead to overall particle accumulation. We defined a threshold whereby stations with integrated subsurface excess exceeding 20% of P ($P_{xsfrac} > 0.2$) indicate overall particle accumulation and were not considered indicative of a Cd-specific accumulation process (Figures 2b and 2c). Crucially, this filtering method means that high subsurface Cd:P is not itself an indicator of particulate Cd accumulation, as a subsurface maximum in Cd:P can be accompanied by P excess above 20% (Figure 2b).

Finally, because the double exponential fits assume that gravitational settling and remineralization are the only processes affecting particles, the accumulation method can only be applied below the euphotic zone. Cd-specific accumulation at or above the euphotic zone depth (median = 200 m; Figure S2 in Supporting Information S1) was not identified. Processes within the euphotic zone are indistinguishable with these methods; all euphotic zone uptake is encompassed within the initial concentrations (C_{ref}, C_{lab}) determined by Equation 2. The euphotic zone depth and sampling resolution thus place limits on how well we can identify the accumulation depth. The minimum identifiable accumulation depth for each station based on the euphotic zone depth and sampling resolution is shown in Figure S3 in Supporting Information S1.

3. Results

3.1. GP15 Particulate Cd and P

Distributions of particulate Cd and P across GP15 generally follow the expected patterns for biomass particles: higher concentrations in productive surface waters and declining concentrations with depth. Notably, surface concentrations are elevated in the Equatorial Pacific and north of ∼40°, reaching their maxima (55.9 pM and 118.6 nM for particulate Cd and P, respectively) in the North Pacific High Nutrient Low Chlorophyll (HNLC) region.

The highest concentrations of particulate Cd in the equatorial region (∼4 pM; Figure 3a) are within the euphotic zone at the top of the oxycline (∼100 m), and an elevated signal persists through the upper 500 m of the water column. The much higher particulate Cd concentrations in the HNLC North Pacific (∼50 pM) peak at the surface and persist through the upper 750 m (Figure S4 in Supporting Information S1). These regions are in stark contrast to the North Pacific subtropical gyre region, where near-surface particulate Cd concentrations are low. Here, subsurface particulate Cd maxima (∼0.6–1.4 pM) are ubiquitous between ∼100 and 300 m. Particulate P concentrations show similar overall patterns to Cd. Particulate P concentrations in the surface HNLC North Pacific (>50 nM, Figure 3b) are generally higher than those in the Equatorial Pacific (∼10–20 nM) and the subtropical gyre (∼5–10 nM). However, unlike particulate Cd, there are rarely subsurface particulate P maxima below 50 m. While elevated particulate P concentrations do not persist below ∼250 m, concentrations do remain above detection throughout most of the section (Table S1 in Supporting Information S1).

Particulate Cd:P varies widely in the euphotic zone (mean depth 140 m, Figure S2 in Supporting Information S1; 0.03–1.47 mmol:mol, Figure 3c). Because Cd:P in the euphotic zone of the open ocean is presumably mediated by biological uptake, Bourne et al. (2018) used a multi-linear regression to euphotic zone depth, silicate

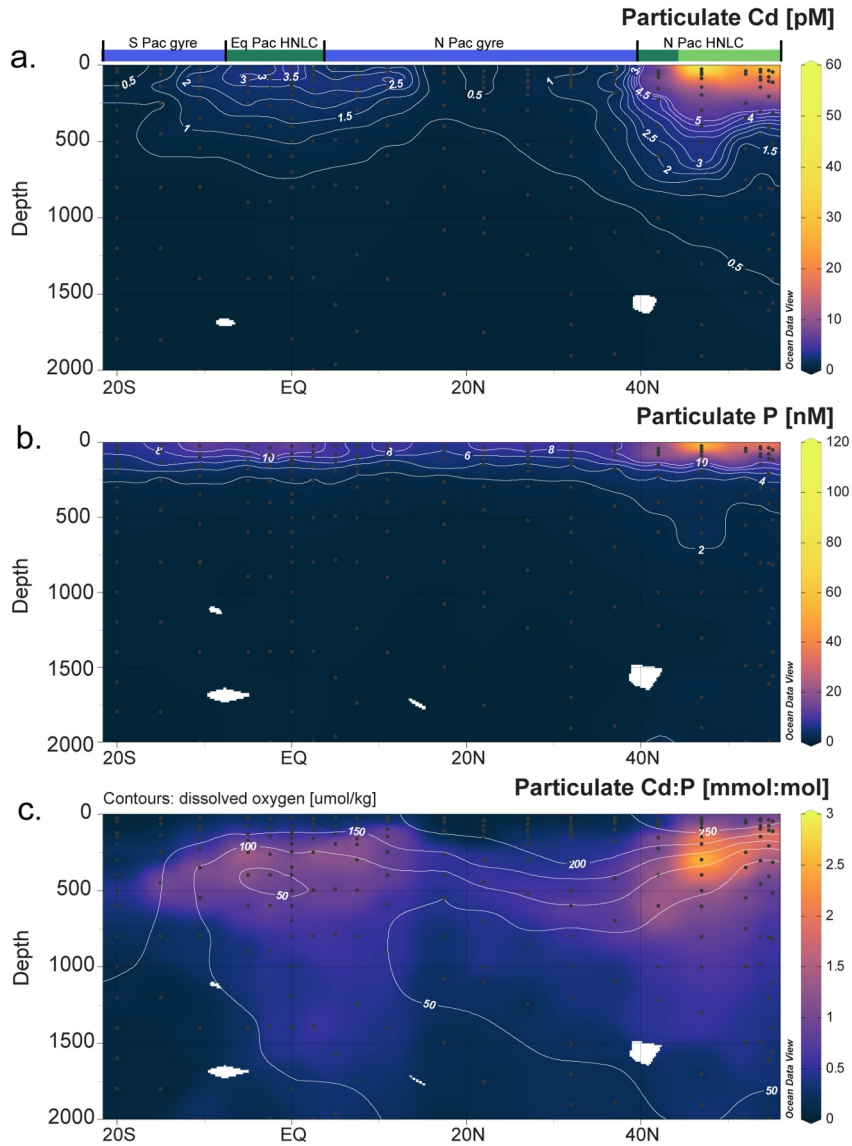

Figure 3. Particulate concentrations across the GP15 transect. (a) Particulate Cd concentrations in pM and (b) particulate P concentrations in nM shown with nonlinear vertical color bar and white contours. (c) Particulate Cd:P shown in mmol:mol with a linear vertical color bar and dissolved oxygen concentration contours in μmol kg^{-1},. The bar at the top of (a) shows the surface nutrient regime associated with each station: low (<0.4 μmol kg^{-1}, blue), moderate (0.4–0.8 μmol kg^{-1}, dark green), and high (>0.8 μmol kg^{-1}, light green).

concentration, and nitrate concentration to make global predictions of surface ocean particulate Cd:P. Across the GP15 transect, station-average euphotic zone particulate Cd:P is highest in the HNLC North Pacific (0.60–0.78 mmol:mol), moderate in the Equatorial Pacific (0.20–0.75 mmol:mol), and lowest in the gyres (0.06–0.23 mmol:mol), a pattern that is less extreme—but broadly similar to—Bourne et al.'s prediction.

Particulate Cd:P peaks in the upper mesopelagic region throughout the transect (Figure 3c), with the highest ratios in the oxyclines (~200–400 m) of the HNLC North Pacific (~1–2.8 mmol:mol) and equatorial regions (~0.7–1.7 mmol:mol). Though particulate Cd:P decreases with depth below ~500 m, relatively high Cd:P (0.15–0.30 mmol:mol) persists through ~4,000 m in these regions. In deep waters, particulate Cd:P is generally low (0.10 ± 0.09 mmol:mol, >4,000 m, $N = 63$, not shown).

3.2. Sensitivity Analysis

The GP16 transect is well-sampled with both a full-profile bottle particulate data set and a pump particulate data set, providing an opportunity to evaluate the sensitivity of the method to two major choices: the use of bottle or pump particulate data, and the excess Cd determination method.

3.2.1. Data Type

There are known discrepancies between bottle and pump particulate data; notably, paired samples have shown insignificant differences in particulate Cd but significantly higher (e.g., up to ~double) particulate P concentrations in bottles (Twining et al., 2015). Our excess point identification method is agnostic toward concentration biases within each profile as long as any potential bias is internally consistent, that is, sampled entirely from bottles or from pumps. However, because of the potential effects of biases in data and differences in sampling frequency on integration, we elect to use either pump or bottle data for each cruise. Full-depth profiles of both bottle and pump particulate data are only available for GP16. Applying the same method to both sets of data, we found particulate Cd accumulation at seven stations using pump data (Cd_{xsfrac} 28%–82%, median = 60%) and nine stations using bottle data (Cd_{xsfrac} 25%–56%, median = 35%; Figure S5 in Supporting Information S1). Four of the stations with Cd accumulation identified in the pump data are outside of the region of Cd accumulation identified using bottle data (Figure S5 in Supporting Information S1). We attribute this to the low incidence of P excess points captured by the pump data (4 out of 132 possible data points) compared to the bottle data (69 out of 364 possible data points), which affects which stations are considered to have Cd-specific accumulation (Figure S6 in Supporting Information S1). Because pump data sets have lower sampling resolution and may miss P and Cd excess, we proceed with bottle data for GP16 assuming the higher sampling resolution favors more precise identification of Cd accumulation.

3.2.2. Excess Cd Identification Method

We used the double-exponential defined in Equation 2 for regeneration fits and refits so that we could account for the presence of more than one "type" of particulate Cd and P with differing lability. To assess the effect of this choice of regeneration parameterization, we compared this method of fitting the data to a regeneration curve and identifying excesses with two other methods of excess identification using GP16 bottle data. First, we followed Section 2.4.2 but used a single exponential equation with a constant (inert) background rather than a double exponential to fit the data. In the single exponential parameterization, all particulate Cd or P beyond the inert background concentration was considered equally labile. Second, we identified excess points qualitatively through visual inspection of each profile, looking for non-monotonic changes in concentration with depth. The qualitative, single exponential, and double exponential methods recorded 121, 86, and 90 depths with particulate Cd excess, respectively. The single exponential method identified four stations with particulate Cd accumulation (Cd_{xsfrac} 44%–55%, median = 50%) compared to nine stations using the double exponential method. Importantly, the particulate Cd excess points identified by each method were similarly distributed throughout the transect both vertically and horizontally (Figure 4), ensuring that their oceanographic interpretations are not sensitive to the method used.

3.3. Regeneration

Of 124 possible stations across the multiple GEOTRACES sections, 19 stations do not have high enough data resolution between the euphotic zone and 2,000 m to complete the depth removal and refit method (Figure 5, gray dots). These stations are excluded from further analysis, leaving 105 total stations. Regeneration alone can describe Cd:P at 10 of these stations, and an additional 19 P profiles and 16 Cd profiles were better fit by the original complete data set regeneration curves than after removal of potential depths with excess particulate Cd or P (Figure 5, open circles). All other stations fit with apparent regeneration equations after the removal of one or more depths with excess particulate Cd or P (Figure 5).

When comparing labile and refractory types of particles, the median [interquartile range] initial concentration of labile P (6.9 nM [3.4–24 nM]) at the base of the euphotic zone is significantly greater than the initial concentration of refractory P overall (2.3 nM [1.1–6.5 nM]; Wilcoxon signed-rank $p < 0.05$) and across each of the three surface nutrient regimes (Table 1, Table S2 in Supporting Information S1). The overall median initial concentration of labile Cd (1.9 pM [0.41–13 pM]) is also significantly greater than refractory Cd ([0.60–3.0 pM]); however, this pattern is reversed in the low surface nutrient regime (e.g., the gyres), where the initial concentration of labile Cd

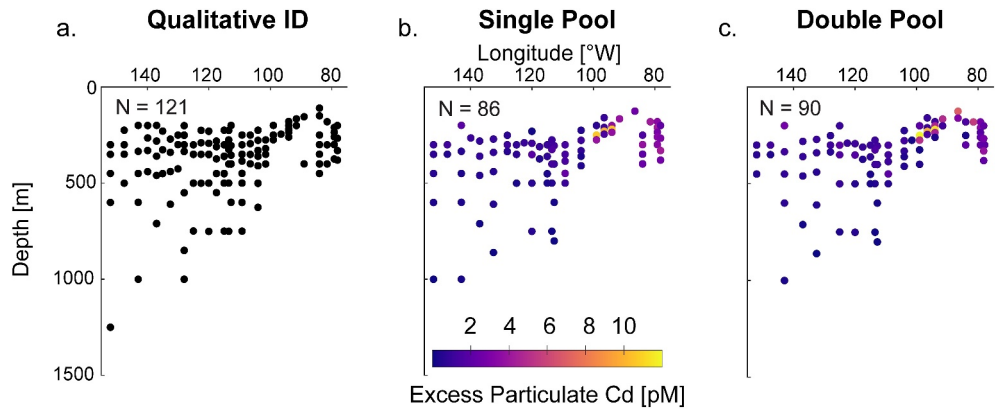

Figure 4. Excess particulate Cd depths were identified for GP16 bottle data using three different methods. Black dots show the location of (a) excess depths identified qualitatively. Color bar shows the magnitude of Cd excess at points identified using a (b) single-pool exponential fit or (c) double-pool exponential fit.

is lower than refractory Cd (0.75 pM [0.13–1.9 pM] and 0.92 pM [0.4–1.4 pM], respectively; Table 1, Table S2 in Supporting Information S1).

The median regeneration length scales of labile P and Cd across all stations are 39 m [19–100 m] and 32 m [7–100 m], respectively, while the median length scales of refractory P and Cd are 650 m [320–960 m] and 620 m [310–940 m], respectively (Table 2, Figure 6). The regeneration length scales of labile Cd and refractory Cd are significantly different from each other (Wilcoxon signed-rank $p < 0.05$, Table S3 in Supporting Information S1), and the regeneration length scales of labile P and refractory P are significantly different from each other in all surface nutrient regimes except high, but the corresponding P and Cd length scales are not statistically distinct from each other (Table S3 in Supporting Information S1). There is high intra-regime and overall variability in the length scale of each pool. The relative variability (interquartile range compared to median) is higher overall in the labile pools (P: 2.1, Cd: 2.9) than in the refractory pools (P: 0.98, Cd: 1.0) but varies across nutrient regimes. Notably, the relative variability in regeneration length scale is high for labile Cd in the low surface nutrient regime (8.9, Table 2). Overall, the regeneration length scales for Cd and P vary between pools and regions, but both labile

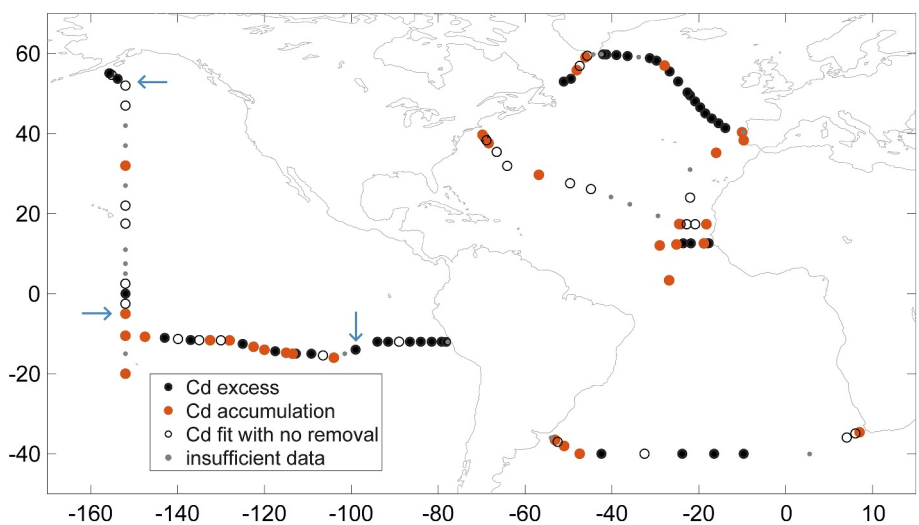

Figure 5. Map of stations with excess particulate Cd (black circles), stations with identified Cd accumulation (orange circles), and stations where Cd is controlled by regeneration only (best fit occurred without removal of any depths; open circles). Fits without depth removal included stations where depth removal was not attempted because initial fits were highly correlated to Cd:P ($R^2 > 0.9$) and stations where after applying the depth removal method the initial regeneration fit still had the lowest root-mean square error. Stations with insufficient data to perform the depth removal method are shown with gray dots. Blue arrows highlight stations also shown in Figure 2.

Table 1
Initial Concentrations of All Apparent Regeneration Pools and Fraction of Each Element That is Initially Partitioned Into the Refractory Pool

Initial concentrations						
Surface phosphate	P_{lab} [nM]	P_{ref} [nM]	Cd_{lab} [pM]	Cd_{ref} [pM]	Frac P_{ref}	Frac Cd_{ref}
Low (<0.4 μmol kg^{-1})	**5.1**	**1.7**	**0.75**	**0.92**	**0.23**	**0.5**
N	58	58	58	58	58	58
25th Percentile	2.4	0.85	0.13	0.4	0.11	0.22
75th Percentile	11	3.7	1.9	1.4	0.35	0.92
IQR/median	1.7	1.7	2.4	1.1	1.0	1.4
Moderate (0.4–0.8 μmol kg^{-1})	**13**	**3.2**	**9.3**	**2.8**	**0.21**	**0.24**
N	37	37	37	37	37	37
25th Percentile	6.2	1.9	2.4	1.6	0.14	0.16
75th Percentile	36	9.7	17	4.4	0.36	0.48
IQR/median	2.3	2.4	1.6	1.0	1.0	1.3
High (>0.8 μmol kg^{-1})	**22**	**6.4**	**17**	**1.4**	**0.22**	**0.07**
N	10	10	10	10	10	10
25th Percentile	6.9	1.5	13	0.86	0.12	0.04
75th Percentile	30	8.2	33	6.3	0.54	0.32
IQR/median	1.1	1.0	1.2	3.9	1.9	4.0
All	**6.9**	**2.3**	**1.9**	**1.3**	**0.21**	**0.34**
N	105	105	105	105	105	105
25th Percentile	3.4	1.1	0.41	0.6	0.12	0.15
75th Percentile	24	6.5	13	3	0.39	0.73
IQR/median	3.0	2.3	6.63	1.82	1.3	1.71

Note. Bold values are medians. All units are as shown, except IQR/median and the fractions refractory, which are unitless.

pools have significantly shallower regeneration length scales than refractory pools. Differences between Cd and P are not as clear as the differences between labile and refractory pools.

Though particulate Cd and P are coarsely linearly correlated in this compiled data set (Figure 7; $R^2 = 0.51$, slope $a = 0.370 \pm 0.008$ SE, $p < 0.0001$), there is considerable variation in the ratio, especially compared to the much stronger global correlation between dissolved Cd and phosphate (e.g., Roshan & DeVries, 2021, Figure S7 in Supporting Information S1). Particulate Cd:P varies across three orders of magnitude both within the euphotic zone (0.001–1.98; median = 0.21 mmol:mol), where variation may be expected due to differences in phytoplankton uptake and stoichiometry (Twining & Baines, 2013), and below the euphotic zone (0.002–6.77; median = 0.29 mmol:mol). This results in nonlinear Cd:P profiles; for example, subsurface Cd:P maxima and secondary maxima are common at stations across all cruise transects. At 45 out of 105 stations, local differences in apparent regeneration of Cd and P cause some of this variability in particulate Cd:P (e.g., Figures 2a and 2c). This variable regeneration effect is seen at stations regardless of whether there is excess Cd or evidence of Cd accumulation, suggesting that both regeneration and accumulation influence the overall observed Cd:P.

3.4. Accumulation

Most stations have depths with excess particulate Cd (75% of 105 stations) or P (72%). As noted in Section 2.4.2, excess and accumulation points cannot be identified within the euphotic zone using our methods. Overall, 19% of particulate Cd measurements and 16% of particulate P measurements between the euphotic zone and 2,000 m are identified as hosting excess metals beyond those fitting the regeneration curves. The median depth of excess particulate elements for Cd (350 m [230–500 m]) and P (300 m [200–430 m]) are similar and within the upper mesopelagic region (Table 3). The median excess concentrations are 0.99 pM [0.46–2.0 pM] and 1.7 nM [0.8–4.7 nM] for Cd and P, respectively (Table 3).

Table 2
Apparent Regeneration Length Scales for All Pools

Regeneration length scales, *m*				
Surface phosphate	P_{lab}	P_{ref}	Cd_{lab}	Cd_{ref}
Low (<0.4 μmol kg^{-1})	**44**	**750**	**21**	**630**
N	56	54	55	53
25th *Percentile*	18	290	4	470
75th *Percentile*	180	1,200	190	850
IQR/median	3.7	1.2	8.9	0.60
Moderate (0.4–0.8 μmol kg^{-1})	**36**	**520**	**40**	**570**
N	36	31	36	33
25th *Percentile*	11	370	11	270
75th *Percentile*	79	820	73	970
IQR/median	1.9	0.9	1.6	1.2
High (>0.8 μmol kg^{-1})	**49**	**370**	**61**	**890**
N	9	8	10	9
25th *Percentile*	33	39	35	200
75th *Percentile*	120	740	120	1,120
IQR/median	1.8	1.9	1.4	1.0
All	**39**	**650**	**32**	**620**
N	100	93	100	95
25th *Percentile*	19	320	7	310
75th *Percentile*	100	960	100	940
IQR/median	2.1	0.98	2.9	1.0

Note. Bold values are medians. All units in meters except for IQR/median, which is unitless. Pools that are functionally inert (length scale >10,000 m; Cd: $N = 14$; P: $N = 16$) are not included.

After excluding stations that also had high excess P (Figure 5, black circles), 31 stations showed evidence of subsurface Cd accumulation (Figure 5, orange circles). Cd accumulation is most densely clustered in the mesopelagic (400 m; Table 3), the Equatorial Pacific, and the Eastern North Atlantic but can be found in every cruise transect. Particulate Cd accumulation is most common at stations in the low surface nutrient regime (N = 23) but is also identified at stations in the moderate surface nutrient regime (N = 8). We do not identify particulate Cd accumulation at any stations in the high surface nutrient regime, despite the presence of excess particulate Cd at many of these stations (N = 7; Figure 5), because excess particulate P is also high at these stations (median $P_{xsfrac} = 0.41$), pointing to a particle-concentration process that is not specific to Cd. Accumulation ranges from 1% to 95% (median = 33% [25%–41%]) of particulate Cd over the depths of incidence at stations where it is identified (Figure 8).

4. Discussion

4.1. GP15 in Context

Dissolved Cd and PO_4 data from GP15 suggest a preferential, yet unexplained, removal of dCd compared to PO_4 in the equatorial mesopelagic (~250–500 m; Sieber et al., 2023b). Here, elevated particulate Cd:P ratios and identified subsurface particulate Cd accumulation at similar depths as these stations provide additional evidence for a local preferential Cd uptake process.

In contrast, dCd data from the HNLC North Pacific region of GP15 show a depletion of dCd near the surface and a surplus at 150–400 m relative to PO_4 (Sieber et al., 2023b; Figure 9e). At these sites, high particulate Cd in the surface, elevated particulate Cd:P from 100 to 400 m, and the absence of identifiable subsurface particulate Cd accumulation suggest a regeneration-dominated paradigm. In agreement with the mechanism proposed by Sieber et al. (2023b), the low surface dCd can be explained by the influence of preferential surface dCd uptake into high-Cd particles that then remineralize in the shallow subsurface and resupply dCd. The preferential Cd uptake at the surface may occur in response to low concentrations of other trace metal micronutrients, as has been suggested in analogous HNLC regions (Abouchami et al., 2014; Baars et al., 2014; Sieber et al., 2019).

Interestingly, the apparent regeneration equations of particulate Cd and P at these stations combine to reproduce a strong subsurface maximum in particulate Cd:P (e.g., Figures 2a). Thus, if the subsurface particulate Cd:P is greater than the surface waters' particulate Cd:P, despite the preferential uptake of Cd into surface cells, then subsurface respiration must be preferentially regenerating P compared to Cd. In the absence of other influences, we would expect a coincident minimum in subsurface dCd:PO_4, as it would replenish relatively more PO_4 than dCd. Instead, the dCd:PO_4 data shows the opposite: a maximum at the same depths in this region (Sieber et al., 2023b; Figure 9e). This suggests that the particulate Cd concentration in cells on the surface of the HNLC North Pacific is sufficiently high to impart an elevated dCd signal in the upper mesopelagic via regeneration despite the preferential regeneration of particulate P occurring at the same depths.

4.2. Cd:P and Variable Regeneration

Both the labile and refractory particulate pools assessed here are considered biogenic, as they are regenerated with depth following the principles of biogenic matter. Because our calculations of regeneration length scales of labile P and Cd are not significantly different, and the length scales of refractory P and Cd are not significantly different, our analysis does not suggest that the two elements are stored in particulate matter pools with inherently different labilities; labile Cd is approximately as labile as labile P; likewise, refractory Cd is approximately as refractory as refractory P (Table 2, Table S3 in Supporting Information S1). Yet, the subsurface maxima in Cd:P suggest variable regeneration. These observations can be explained by differences in the partitioning of particulate Cd and P into the

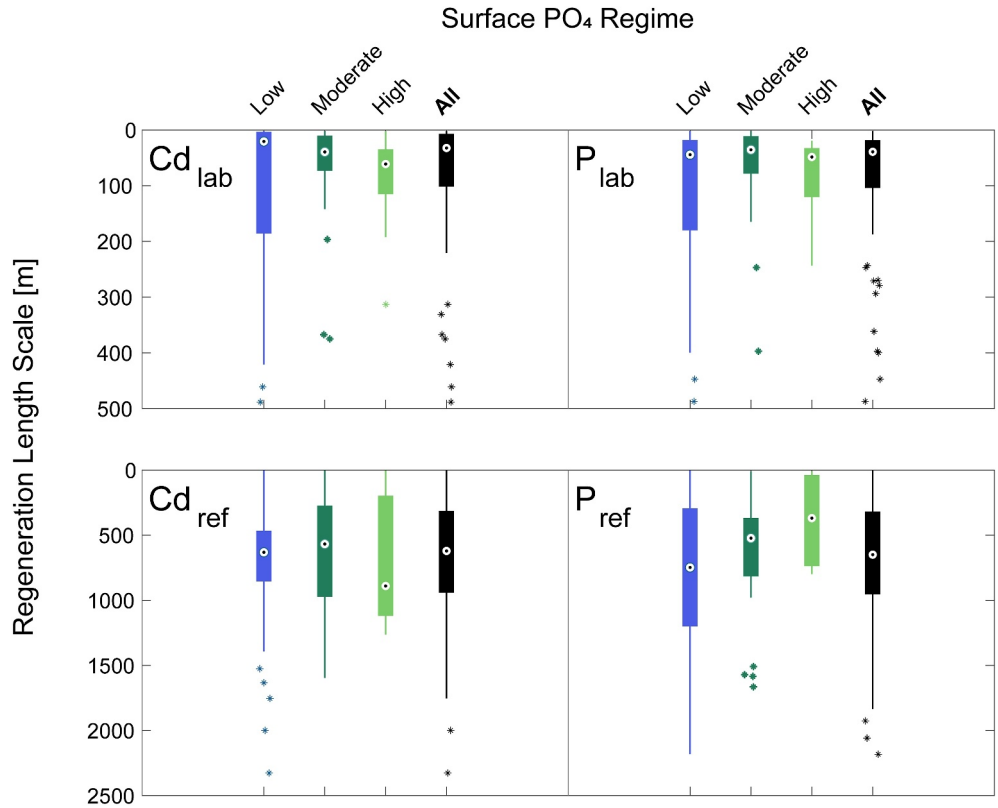

Figure 6. Boxplots depicting regeneration length scales for each pool in different surface nutrient regimes and overall. Pools that are functionally inert (length scale >10,000 m; Cd: N = 12; P: N = 16) are not included. Some outliers are off panel (Cd_{lab}: N = 9; P_{lab}: N = 6; Cd_{ref}: N = 2; P_{ref}: N = 4). For the number of stations in each pool, see Table 1.

refractory pool. The fraction of the total initial Cd concentration in the refractory pool (34%) is significantly higher than the fraction of the total initial P concentration in the refractory pool (21%, Table 1, Table S2 in Supporting Information S1). As the different pools are regenerated with depth, the relative partitioning into the refractory pool changes. The labile pools regenerate over a short length scale, becoming less dominant with depth. Eventually, the

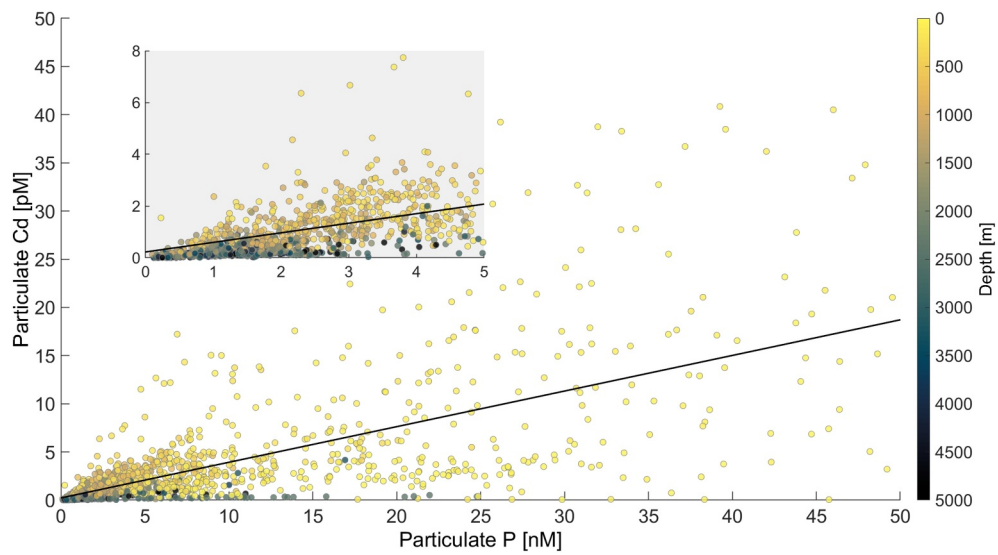

Figure 7. Correlation between particulate Cd and P concentrations for all data included in our compilation (stations are shown in Figure 1), colored by depth. Inset panel zooms in on concentrations less than 8 pM and 5 nM of Cd and P, respectively.

Table 3
Excess Point and Cd Accumulation Depths and Concentrations

Excess points	P excess	Cd excess	Cd accumulation
Depth	**300**	**350**	**400**
N	*191*	*236*	85
25th Percentile	200	230	300
75th Percentile	430	500	600
IQR/median	0.77	0.78	0.75
Concentration	**1.7**	**0.99**	**0.60**
N	*191*	*236*	85
25th Percentile	0.80	0.46	0.38
75th Percentile	4.7	2.0	1.2
IQR/median	2.3	1.6	1.4

Note. Bold values are medians. All depths given in meters. P excess concentrations are in nM; Cd excess and Cd accumulation concentrations are in pM. Excess and accumulation concentrations are calculated point-wise as offset from apparent regeneration fit.

remaining particulate material is dominated by the refractory pool. The depth at which this occurs depends on both the regeneration length scales and the initial partitioning into the refractory pool. A station with median initial concentrations and regeneration length scales would have particulate Cd and P nearly entirely (>99%) partitioned into the refractory pool by ∼170 and ∼240 m below the euphotic zone, respectively. The *overall* lability of particulate Cd or P therefore varies with depth as a function of the partitioning between pools. This suggests a depth-dependence to the variation in regeneration between particulate Cd and P, rather than a constant regeneration ratio.

The apparent regeneration length scales derived here bookend those predicted for a single pool by Roshan and DeVries (2021): the labile length scale (∼35 m below euphotic zone) is shorter than their prediction (Cd ∼ 450 m; P ∼ 390 m) and the refractory length scale (∼640 m below euphotic zone) is longer than their prediction. They also predict a Cd:P regeneration ratio that varies with depth. Thus, their model could simulate the overall regeneration of both pools combined.

4.3. Cd Accumulation

Evidence of particulate Cd accumulation is seen most consistently in the tropical Pacific (Figures 5 and 8) where it aligns with regions of low dCd:PO_4 (Figures 9e and 9f). Our identification of Cd accumulation in this region supports previous arguments for a loss of dCd to the particle phase between ∼200 and 600 m by Ohnemus et al. (2019) and ∼200–400 m by de Souza et al. (2022) in their analyses of the GP16 transect. Interestingly, however, we also find evidence of particulate Cd accumulation outside the tropics. We thus hypothesize that the Cd accumulation process is not unique to low latitude oxyclines but may also occur in other regions where it is not easily resolvable in dCd observations due to its small contribution to the dCd budget compared to the larger influences of, for example, water mass mixing. Our analysis here cannot pinpoint the mechanism of this Cd accumulation process; however, patterns in identifiable particulate Cd accumulation can help support or refute hypothesized mechanisms.

4.3.1. Oxygen and Acid Volatile Sulfides

Early hypotheses for a particulate Cd accumulation process suggested that precipitation of CdS in oxygen minimum zones or sinking particle microenvironments might explain dCd and PO_4 decoupling (Bianchi et al., 2018; Janssen et al., 2014). Since then, the role of CdS precipitation in setting global dCd:PO_4 patterns has been the subject of debate (de Souza et al., 2022), and previous studies of oxygen deficient zones in GP16 and the Kuroshio-

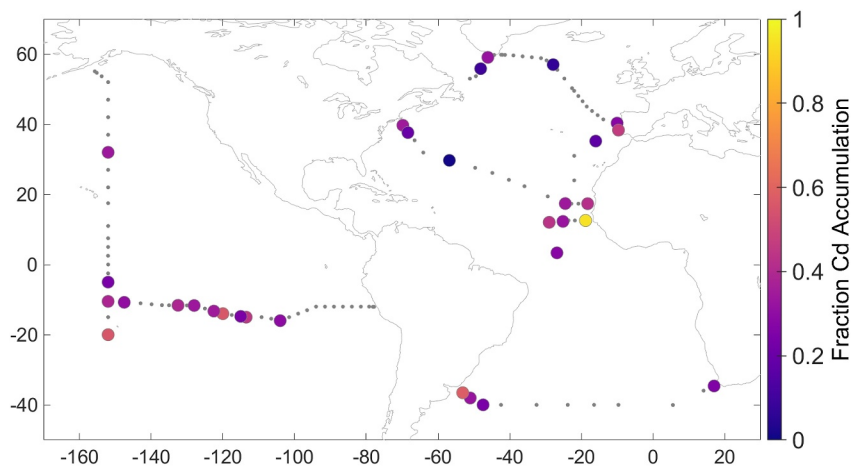

Figure 8. Map of stations with identified Cd-specific accumulation. Stations are colored according to the fraction of particulate Cd attributed to Cd accumulation over the depths of incidence (Cd_{xsfrac}). All other station locations are shown in smaller gray dots.

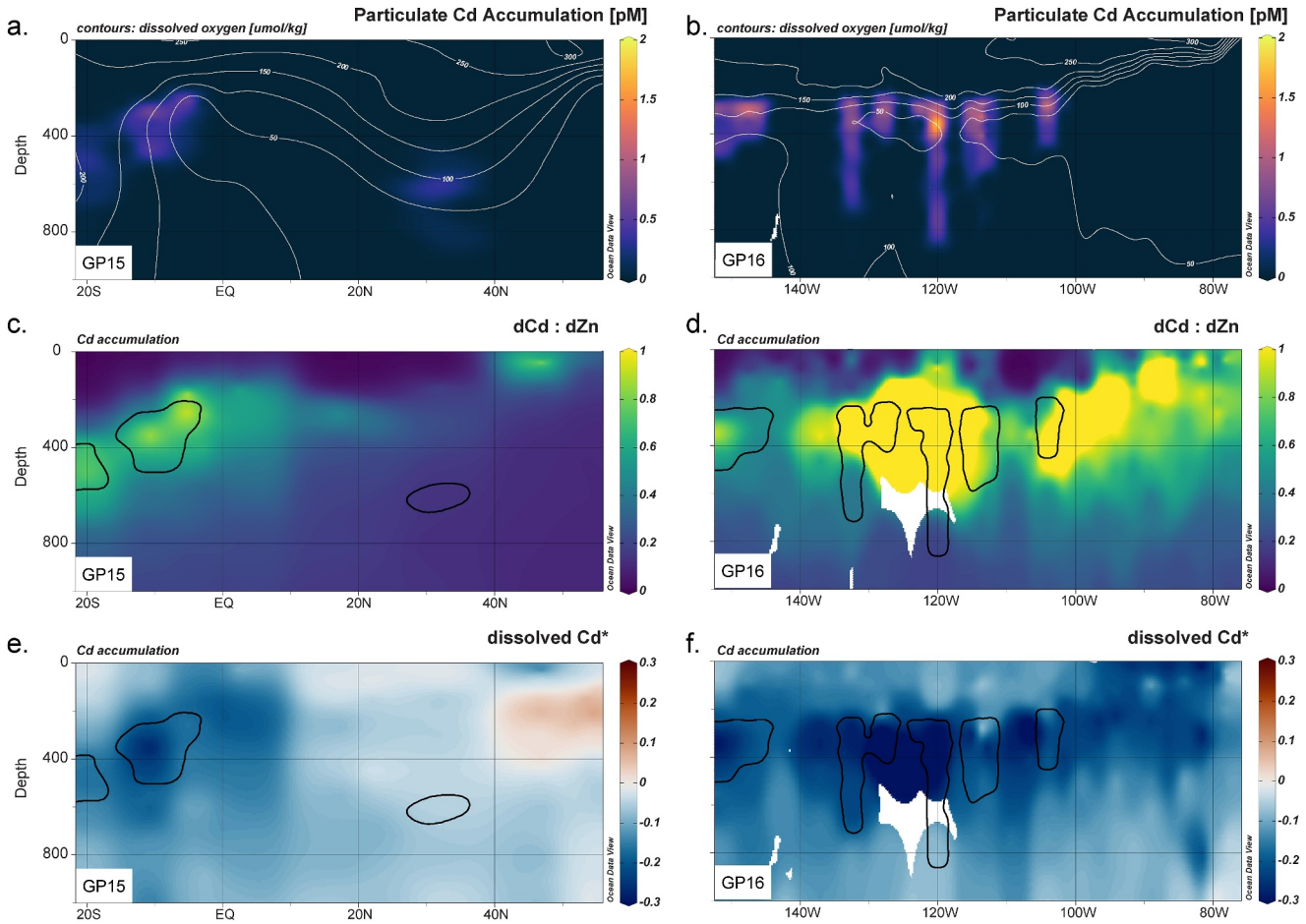

Figure 9. Section plots showing identified Cd accumulation across (a, c, and e) GP15 and (b, d, and f) GP16. Stations east of 100W in GP16 often have excess particulate Cd (Figure 5) but are not considered Cd-specific accumulation because excess particulate P is also high (Figure S6 in Supporting Information S1). Methodological constraints limit detection of Cd accumulation in this region below ~200 m (Figure S3 in Supporting Information S1). Particulate Cd accumulation in pM (a, b) with contours showing dissolved oxygen concentration in μmol kg^{-1},. Ratio of dCd to dZn (c, d) with contours showing particulate Cd accumulation incidence. Calculated Cd* (e, f) with contours showing particulate Cd accumulation incidence. We calculate Cd* following Janssen et al. (2014), where Cd* is the deviation in dCd:PO_4 relative to a reference ratio of 0.35 mmol:mol.

Oyashio Extension do not show dCd deficiency (John et al., 2018; Yang et al., 2018). We find that dissolved oxygen is not well-correlated with excess particulate Cd ($R^2 = 0.02$, $p = 0.07$) or identified Cd accumulation ($R^2 = 0.08$, $p = 0.015$). Further, particulate Cd accumulation is not confined to oxygen minimum zones or low-oxygen waters (Figures 9a and 9b), suggesting that it is not driven exclusively by low ambient dissolved oxygen concentrations.

In a recent analysis of particulate acid volatile sulfide concentrations (pAVS), which include CdS and other sulfides, Buckley et al. (2024) found maximum pAVS in the shallow subsurface (<250 m) of stations from GP15 and GP16. These maxima are shallower than regions of identified Cd accumulation in our study (Figure 9) and were largely attributed to sulfide produced during assimilatory sulfate reduction during photosynthesis along GP15. For the GP16 transect, Buckley et al. (2024) asserted that pAVS could contribute to the decoupling of dCd:PO_4 but cannot account for the full removal of dCd at all stations. They reported especially elevated pAVS in the eastern part of the section (east of 100W), where we found particulate Cd excess but not accumulation (Figure 5). In a region where we do find particulate Cd accumulation (110–120W), Buckley et al. (2024) found elevated pAVS throughout the upper 500 m, likely related to both assimilatory and dissimilatory sulfate reduction. Due to the depth limitations of our methods, however, we cannot identify Cd accumulation at depths shallower than ~200 m (Figure S3 in Supporting Information S1), so we are unable to identify CdS precipitation related to assimilatory sulfides in surface waters. However, at the depths where we can apply our methods, we find no

significant correlation between pAVS and excess particulate Cd from the same pump filters (N = 21; $p = 0.74$); thus, we conclude that an alternative process is needed to explain Cd-specific accumulation into particles at depth.

4.3.2. Dissolved Trace Metals and Mesopelagic Uptake

Enhanced Cd uptake by phytoplankton in the euphotic zone has been linked to high concentrations of dCd (Twining & Baines, 2013) and low dissolved concentrations of other divalent bioactive trace metals, notably Fe and Zn (Cullen et al., 2003; Cullen & Sherrell, 2005; Lane et al., 2009; Sunda & Huntsman, 2000). Cd uptake in response to low Fe concentrations may be nonspecific (Horner et al., 2013) as Cd is not known to alleviate Fe stress. In contrast, Cd can substitute for Zn in the carbonic anhydrase enzyme (Lane & Morel, 2000; Xu et al., 2007) and can partially alleviate Zn stress (Cox & Saito, 2013; Lee & Morel, 1995). Cd uptake may therefore be expected to be elevated when dCd concentrations are high compared to dZn and when carbon fixation rates, and thus the requirement for carbonic anhydrase, are high (Morel et al., 2020).

To our knowledge, the substitution of Cd for other trace metals in the mesopelagic has not been studied. Dissolved Cd and dZn both increase with depth, but this increase generally occurs closer to the surface for dCd than dZn. In both GP15 (Sieber et al., 2023a, 2023b) and GP16 (John et al., 2018), depths of high dCd:dZn often coincide with identified Cd accumulation (Figures 9c and 9d). Building on the ideas of Ohnemus et al. (2017, 2019), we hypothesize that in the mesopelagic region, as in the surface, a biological uptake mechanism is driving the Cd accumulation process in response to this balance of dissolved trace metals. As hydrocarbon-degrading marine bacterial activity has been shown to be stimulated by Fe and Zn additions (Baltar et al., 2018), and recent work has shown evidence for mesopelagic Fe limitation (Li et al., 2024), we further speculate that particle-associated microbes (Baltar et al., 2009) may be driving subsurface Cd accumulation in response to micronutrient stress. More work is necessary to conclusively link mesopelagic pCd and Zn demand.

5. Limitations

This work is limited primarily by the steady-state, one-dimensional assumption necessary for the apparent regeneration equation fits. There are several processes that do not fit this assumption, including the effects of lateral transport processes, diel vertical migration, and temporal variability in production. While particles do not have the same long "memory" as water masses, the slow sinking speed of small particles (~0.4–1 m d^{-1}; Amaral et al., 2024; Xiang et al., 2022) means that the particles assessed here have likely been in the water column for timescales of months to years and may thus record temporal variation. All of these processes could contribute to points of excess Cd and P within individual station profiles, and we attempted to differentiate between general particulate excess and Cd-specific accumulation through our application of the depth removal method to particulate P. Still, despite a conservative effort to discount stations with >20% excess particulate P for the positive identification of particulate Cd accumulation, we cannot fully exclude the influence of these other processes.

6. Conclusions

In this study, we apply a simple depth-removal algorithm to particulate Cd and P data to identify locations with evidence of subsurface particulate Cd accumulation. Using fits to double exponential decay equations at each station, we characterize the apparent regeneration of labile and refractory pools of particulate Cd and P. We present and include new particulate data from the GEOTRACES Pacific Meridional Transect, GP15.

Compiled particulate Cd and P are more poorly correlated compared to the strong correlation between dissolved Cd and PO_4 (Figure S7 in Supporting Information S1), resulting in highly variable Cd:P. Individual profiles often have a subsurface maximum in Cd:P, which is thought to be explained in part by variable regeneration of Cd and P (Bourne et al., 2018). The apparent regeneration parameters derived here suggest that variable Cd:P regeneration can at least partially explain subsurface Cd:P maxima at many stations and is driven by differences in the fraction of each element that is partitioned into the refractory pool.

At some stations with excess particulate Cd, variable regeneration alone does not explain the elevated Cd:P, and mesopelagic particulate Cd accumulation must be invoked. We find evidence of subsurface particulate Cd accumulation at 31 out of 105 stations, representing every cruise transect in the data compilation. While particulate Cd accumulation is most coherently clustered in the equatorial Pacific, where it was predicted based on dCd analyses (Figures 9e and 9f), we hypothesize that it is driven by a more ubiquitous mesopelagic process that

may not be easily resolvable in dCd data. We note that the typical depth of excess Cd and identified Cd accumulation falls near the cutoff depth (~300 m) used to differentiate between uptake-driven surface dCd dynamics and regeneration and circulation driven deep water dCd dynamics (Roshan & Wu, 2015; Matthias Sieber et al., 2023b), potentially obfuscating its visibility in dCd analyses.

Though typically located in oxyclines, subsurface particulate Cd accumulation is not well correlated with dissolved oxygen concentration or pAVS, suggesting that it is not primarily due to CdS precipitation. We find that particulate Cd accumulation in the equatorial Pacific also coincides with regions of relatively high dCd compared to dZn and hypothesize that accumulation could be the result of enhanced biological Cd uptake in the mesopelagic, perhaps in response to the subsurface trace metal micronutrient balance.

Our analysis lends support to the proposed loss of dCd to the particle phase in the upper mesopelagic Equatorial Pacific and suggests that this process also occurs in other regions. Individual particulate Cd:P profiles can be described through a combination of the effects of variable regeneration and this subsurface particulate Cd accumulation feature. Though this study improves our understanding of the linkages between particulate and dCd observations, more work is needed to conclusively identify the drivers and mechanisms of the particulate Cd accumulation process. Specifically, studies exploring potential subsurface micronutrient stress and the balance of dissolved trace metals in the mesopelagic will improve our understanding of possible enhanced biological trace metal uptake.

Data Availability Statement

Particulate Cd and P data from the GP15 transect can be downloaded from the Biological and Chemical Oceanography Data Management Office (BCO-DMO; Lam et al., 2024a, 2024b). The dissolved Cd and Zn data from GP15 are combined measurements from USF, USC, and TAMU as reported by Sieber et al. (2023a, 2023b), respectively. The USF dataset is currently available on BCO-DMO (Conway et al., 2022a, 2022b). Additional data from GP15: particulate sulfide (Cutter & Buckley, 2022a, 2022b). Data from GP16: dissolved Fe, Cd, Zn (Wu, 2017); particulate sulfide (Cutter, 2020); pump particle concentrations (Lam, 2017); bottle particle concentrations (Sherrell et al., 2016). Data from GA03: dissolved Fe, Cd, Zn (John, 2016) and pump particle concentrations (Lam, 2018). Data from GA01, GA06, and GA10 are available via the GEOTRACES Intermediate Data Product (2023). An example implementation of the depth removal and fitting algorithm used in this manuscript is available (Laubach, 2024). Ocean Data View (Schlitzer, 2023) was used to produce Figures 3 and 9, Figures S1 and S4 in Supporting Information S1.

Acknowledgments
We thank the captain, crew, and science team aboard the R/V *Roger Revelle* during the GP15 transect for their work collecting dissolved and particulate samples. We are grateful to the international GEOTRACES community for contributing data to the compilation and to the NASA MODIS mission scientists for their work producing the mapped satellite data products used in this study. Thanks to N. R. Buckley and G. A. Cutter for sharing pAVS data. We also thank two anonymous reviewers for their comments, which helped improve this manuscript. The International GEOTRACES Program is possible in part thanks to the support from NSF Grant OCE-2140395 to the Scientific Committee on Oceanic Research (SCOR). This work was supported by NSF Grants OCE-1657781 and OCE-1736601 to P. J. Lam, OCE-1737136 to T. M Conway, OCE-1737167 to J. N. Fitzsimmons, and GRFP-1746932 to N. T. Lanning.

References

Abouchami, W., Galer, S. J. G., de Baar, H. J. W., Middag, R., Vance, D., Zhao, Y., et al. (2014). Biogeochemical cycling of cadmium isotopes in the Southern Ocean along the zero meridian. *Geochimica et Cosmochimica Acta*, *127*, 348–367. https://doi.org/10.1016/j.gca.2013.10.022

Amaral, V. J., Lam, P. J., Marchal, O., & Kenyon, J. A. (2024). Cycling rates of particulate organic carbon along the GEOTRACES Pacific Meridional transect GP15. *Global Biogeochemical Cycles*, *38*(1), e2023GB007940. https://doi.org/10.1029/2023GB007940

Baltar, F., Arístegui, J., Gasol, J. M., Sintes, E., & Herndl, G. J. (2009). Evidence of prokaryotic metabolism on suspended particulate organic matter in the dark waters of the subtropical North Atlantic. *Limnology and Oceanography*, *54*(1), 182–193. https://doi.org/10.4319/lo.2009.54.1.0182

Baars, O., Abouchami, W., Galer, S. J. G., Boye, M., & Croot, P. L. (2014). Dissolved cadmium in the Southern Ocean: Distribution, speciation, and relation to phosphate. *Limnology & Oceanography*, *59*(2), 385–399. https://doi.org/10.4319/lo.2014.59.2.0385

Baltar, F., Gutiérrez-Rodríguez, A., Meyer, M., Skudelny, I., Sander, S., Thomson, B., et al. (2018). Specific effect of trace metals on marine heterotrophic microbial activity and diversity: Key role of iron and zinc and hydrocarbon-degrading bacteria. *Frontiers in Microbiology*, *9*. https://doi.org/10.3389/fmicb.2018.03190

Bianchi, D., Weber, T. S., Kiko, R., & Deutsch, C. (2018). Global niche of marine anaerobic metabolisms expanded by particle microenvironments. *Nature Geoscience*, *11*(4), 263–268. https://doi.org/10.1038/s41561-018-0081-0

Black, E. E., Lam, P. J., Lee, J.-M., & Buesseler, K. O. (2019). Insights from the 238U-234Th method into the coupling of biological export and the cycling of cadmium, cobalt, and manganese in the Southeast Pacific Ocean. *Global Biogeochemical Cycles*, *33*(1), 15–36. https://doi.org/10.1029/2018GB005985

Bourne, H. L., Bishop, J. K. B., Lam, P. J., & Ohnemus, D. C. (2018). Global spatial and temporal variation of Cd:P in euphotic zone particulates. *Global Biogeochemical Cycles*, *32*(7), 1123–1141. https://doi.org/10.1029/2017GB005842

Boyle, E. A., Sclater, F., & Edmond, J. M. (1976). On the marine geochemistry of cadmium. *Nature*, *263*(5572), 42–44. https://doi.org/10.1038/263042a0

Brand, L. E., Sunda, W. G., & Guillard, R. R. L. (1986). Reduction of marine phytoplankton reproduction rates by copper and cadmium. *Journal of Experimental Marine Biology and Ecology*, *96*(3), 225–250. https://doi.org/10.1016/0022-0981(86)90205-4

Bridgestock, L., Rehkämper, M., van de Flierdt, T., Paul, M., Milne, A., Lohan, M. C., & Achterberg, E. P. (2018). The distribution of lead concentrations and isotope compositions in the Eastern Tropical Atlantic Ocean. *Geochimica et Cosmochimica Acta*, *225*, 36–51. https://doi.org/10.1016/j.gca.2018.01.018

Bruland, K. W., Knauer, G. A., & Martin, J. H. (1978). Cadmium in northeast Pacific waters 1. *Limnology & Oceanography*, *23*(4), 618–625. https://doi.org/10.4319/lo.1978.23.4.0618

Buckley, N. R., Black, E. E., Kenyon, J. A., Lanning, N. T., Sieber, M., Conway, T. M., et al. (2024). Re-evaluating hydrogen sulfide as a sink for cadmium and zinc in the oxic to suboxic upper water column of the Pacific Ocean. *Global Biogeochemical Cycles*, *38*(3), e2023GB007881. https://doi.org/10.1029/2023GB007881

Chen, X.-G., Gledhill, M., Lohan, M. C., Milne, A., & Achterberg, E. P. (2024). Surface ocean biogeochemistry and deep ocean circulation control relationships between nutrient-type trace metals (Cd, Ni, Cu, and Zn) and nutrients in the South Atlantic Ocean near the subtropical front. *Geochimica et Cosmochimica Acta*, *370*, 144–160. https://doi.org/10.1016/j.gca.2024.01.001

Conway, T. M., & John, S. G. (2015). Biogeochemical cycling of cadmium isotopes along a high-resolution section through the North Atlantic Ocean. *Geochimica et Cosmochimica Acta*, *148*, 269–283. https://doi.org/10.1016/j.gca.2014.09.032

Conway, T. M., John, S. G., & Sieber, M. (2022a). Dissolved concentrations and stable isotope ratios of Fe, Zn, and Cd from leg 1 (Seattle, WA to Hilo, HI) of the US GEOTRACES Pacific Meridional Transect (PMT) cruise (GP15, RR1814) on R/V Roger Revelle from September to October 2018 [Dataset]. *Biological and Chemical Oceanography Data Management Office (BCO-DMO)*. https://doi.org/10.26008/1912/bco-dmo.883862.1

Conway, T. M., John, S. G., & Sieber, M. (2022b). Dissolved concentrations and stable isotope ratios of Fe, Zn, and Cd from leg 2 (Hilo, HI to Papeete, French Polynesia) of the US GEOTRACES Pacific Meridional Transect (PMT) cruise (GP15, RR1815) on R/V Roger Revelle from October to November 2018 [Dataset]. *Biological and Chemical Oceanography Data Management Office (BCO-DMO). (Version 1) Version Date 2022-12-06*. https://doi.org/10.26008/1912/bco-dmo.884673.1

Conway, T. M., & Middag, R. (2024). Controls and distributions of trace elements in the ocean. In *Treatise of Geochemistry* (3rd ed.). In Press.

Cox, A., & Saito, M. (2013). Proteomic responses of oceanic Synechococcus WH8102 to phosphate and zinc scarcity and cadmium additions. *Frontiers in Microbiology*, *4*. https://doi.org/10.3389/fmicb.2013.00387

Cullen, J. T., Chase, Z., Coale, K. H., Fitzwater, S. E., & Sherrell, R. M. (2003). Effect of iron limitation on the cadmium to phosphorus ratio of natural phytoplankton assemblages from the Southern Ocean. *Limnology & Oceanography*, *48*(3), 1079–1087. https://doi.org/10.4319/lo.2003.48.3.1079

Cullen, J. T., & Sherrell, R. M. (2005). Effects of dissolved carbon dioxide, zinc, and manganese on the cadmium to phosphorus ratio in natural phytoplankton assemblages. *Limnology & Oceanography*, *50*(4), 1193–1204. https://doi.org/10.4319/lo.2005.50.4.1193

Cutter, G. (2020). Particulate Acid-Volatile Sulfide (pAVS) and Elemental Selenium (pSe) concentrations from a McLane pump collected during the R/V Thomas G. Thompson cruise TN303 from Peru to Tahiti in 2013 (U.S. GEOTRACES EPZT project) [Dataset]. *Biological and Chemical Oceanography Data Management Office (BCO-DMO)*. https://doi.org/10.26008/1912/bco-dmo.646143.1

Cutter, G. A., & Buckley, N. R. (2022a). Particulate Acid-Volatile Sulfide (pAVS) and Chromium Reducible Sulfide (pCRS) from Leg 1 (Seattle, WA to Hilo, HI) of the US GEOTRACES Pacific Meridional transect (PMT) cruise (GP15, RR1814) on R/V Roger Revelle from September to October 2018 [Dataset]. *Biological and Chemical Oceanography Data Management Office (BCO-DMO)*. https://doi.org/10.26008/1912/bco-dmo.873765.1

Cutter, G. A., & Buckley, N. R. (2022b). Particulate Acid-Volatile Sulfide (pAVS) and Chromium Reducible Sulfide (pCRS) from Leg 2 (Hilo, HI to Papeete, French Polynesia) of the US GEOTRACES Pacific Meridional Transect (PMT) Cruise (GP15, RR1815) on R/V Roger Revelle from Oct to Nov 2018 [Dataset]. *Biological and Chemical Oceanography Data Management Office (BCO-DMO)*. https://doi.org/10.26008/1912/bco-dmo.873792.1

de Baar, H. J. W., Saager, P. M., Nolting, R. F., & van der Meer, J. (1994). Cadmium versus phosphate in the World Ocean. *Marine Chemistry*, *46*(3), 261–281. https://doi.org/10.1016/0304-4203(94)90082-5

de Souza, G. F., Vance, D., Sieber, M., Conway, T. M., & Little, S. H. (2022). Re-assessing the influence of particle-hosted sulphide precipitation on the marine cadmium cycle. *Geochimica et Cosmochimica Acta*, *322*, 274–296. https://doi.org/10.1016/j.gca.2022.02.009

Fitzsimmons, J. N., John, S. G., Marsay, C. M., Hoffman, C. L., Nicholas, S. L., Toner, B. M., et al. (2017). Iron persistence in a distal hydrothermal plume supported by dissolved–particulate exchange. *Nature Geoscience*, *10*(3), 195–201. https://doi.org/10.1038/ngeo2900

Fitzsimmons, J. N., & Steffen, J. M. (2024). The "net" impact of hydrothermal venting on oceanic elemental inventories: Contributions to plume geochemistry from the international GEOTRACES program. *Oceanography*, *37*(2), 102–115. https://doi.org/10.5670/oceanog.2024.421

Frew, R. D., & Hunter, K. A. (1992). Influence of Southern Ocean waters on the cadmium–phosphate properties of the global ocean. *Nature*, *360*(6400), 144–146. https://doi.org/10.1038/360144a0

Garcia, H. E., Bouchard, C., Cross, S. L., Paver, C. R., Wang, Z., Reagan, J. R., et al. (2024). In A. Mishonov (Ed.), *World Ocean Atlas 2023, volume 4: Dissolved Inorganic nutrients (Phosphate, Nitrate, Silicate)*. NOAA Atlas NESDIS 92.

GEOTRACES Intermediate Data Product Group. (2023). *The GEOTRACES intermediate data product 2021v2 (IDP2021v2)*. NERC EDS British Oceanographic Data Centre NOC. https://doi.org/10.5285/ff46f034-f47c-05f9-e053-6c86abc0dc7e

Gerringa, L. J. A., Rijkenberg, M. J. A., Slagter, H. A., Laan, P., Paffrath, R., Bauch, D., et al. (2021). Dissolved Cd, Co, Cu, Fe, Mn, Ni, and Zn in the Arctic Ocean. *Journal of Geophysical Research: Oceans*, *126*(9), e2021JC017323. https://doi.org/10.1029/2021JC017323

Gourain, A., Planquette, H., Cheize, M., Lemaitre, N., Menzel Barraqueta, J.-L., Shelley, R., et al. (2019). Inputs and processes affecting the distribution of particulate iron in the North Atlantic along the GEOVIDE (GEOTRACES GA01) section. *Biogeosciences*, *16*(7), 1563–1582. https://doi.org/10.5194/bg-16-1563-2019

Guinoiseau, D., Galer, S. J. G., & Abouchami, W. (2018). Effect of cadmium sulphide precipitation on the partitioning of Cd isotopes: Implications for the oceanic Cd cycle. *Earth and Planetary Science Letters*, *498*, 300–308. https://doi.org/10.1016/j.epsl.2018.06.039

Gutierrez-Mejia, E., Lares, M. L., Huerta-Diaz, M. A., & Delgadillo-Hinojosa, F. (2016). Cadmium and phosphate variability during algal blooms of the dinoflagellate *Lingulodinium polyedrum* in Todos Santos Bay, Baja California, Mexico. *The Science of the Total Environment*, *541*, 865–876. https://doi.org/10.1016/j.scitotenv.2015.09.081

Hernández-Candelario, I. C., Lares, M. L., Camacho-Ibar, V. F., Linacre, L., Gutiérrez-Mejía, E., & Pérez-Brunius, P. (2019). Dissolved cadmium and its relation to phosphate in the deep region of the Gulf of Mexico. *Journal of Marine Systems*, *193*, 27–45. https://doi.org/10.1016/j.jmarsys.2019.01.005

Ho, T.-Y., Quigg, A., Finkel, Z. V., Milligan, A. J., Wyman, K., Falkowski, P. G., & Morel, F. M. M. (2003). The elemental composition of some marine Phytoplankton1. *Journal of Phycology*, *39*(6), 1145–1159. https://doi.org/10.1111/j.0022-3646.2003.03-090.x

Horner, T. J., Lee, R. B. Y., Henderson, G. M., & Rickaby, R. E. M. (2013). Nonspecific uptake and homeostasis drive the oceanic cadmium cycle. *Proceedings of the National Academy of Sciences* (Vol. 110(7), 2500–2505). https://doi.org/10.1073/pnas.1213857110

Janssen, D. J., Conway, T. M., John, S. G., Christian, J. R., Kramer, D. I., Pedersen, T. F., & Cullen, J. T. (2014). Undocumented water column sink for cadmium in open ocean oxygen-deficient zones. *Proceedings of the National Academy of Sciences* (Vol. 111(19), 6888–6893). https://doi.org/10.1073/pnas.1402388111

John, S. G. (2016). Dissolved Fe, Zn and Cd concentrations and isotope ratios from R/V Knorr KN199-04, KN204-01 in the subtropical North Atlantic Ocean from 2010-2011 (U.S. GEOTRACES NAT project) [Dataset]. *Biological and Chemical Oceanography Data Management Office (BCO-DMO)*. http://lod.bco-dmo.org/id/dataset/3840

John, S. G., Helgoe, J., & Townsend, E. (2018). Biogeochemical cycling of Zn and Cd and their stable isotopes in the eastern tropical South Pacific. *Marine Chemistry*, *201*, 256–262. https://doi.org/10.1016/j.marchem.2017.06.001

Lam, P. (2017). Size-fractionated major and minor particle composition and concentration collected from RV Thompson (TN303) along the US GEOTRACES EPZT transect in the Eastern Tropical Pacific during 2013 (US GEOTRACES EPZT project) [Dataset]. *Biological and Chemical Oceanography Data Management Office (BCO-DMO)*. https://doi.org/10.1575/1912/bco-dmo.668083.1

Lam, P. (2018). Size-fractionated major and minor particle composition and concentration from R/V Knorr KN199-04, KN204-01 in the subtropical North Atlantic Ocean from 2010-2011 (U.S. GEOTRACES NAT project) [Dataset]. *Biological and Chemical Oceanography Data Management Office (BCO-DMO)*. https://doi.org/10.1575/1912/bco-dmo.3871.5.1

Lam, P. J., Lee, J., Amaral, V. J., Laubach, A., Carracino, N., Rojas, S., & Mateos, K. (2024a). Size-fractionated major, minor, and trace particle composition and concentration from Leg 1 (Seattle, WA to Hilo, HI) of the US GEOTRACES Pacific Meridional transect (PMT) cruise (GP15, RR1814) on R/V Roger Revelle from Sept to Oct 2018 [Dataset]. *Biological and Chemical Oceanography Data Management Office (BCO-DMO)*. https://doi.org/10.26008/1912/bco-dmo.918811.1

Lam, P. J., Lee, J., Amaral, V. J., Laubach, A., Carracino, N., Rojas, S., & Mateos, K. (2024b). Size-fractionated major, minor, and trace particle composition and concentration from Leg 2 (Hilo, HI to Papeete, French Polynesia) of the US GEOTRACES Pacific Meridional transect (PMT) cruise (GP15, RR1815) on R/V Roger Revelle from Oct to Nov 2018 [Dataset]. *Biological and Chemical Oceanography Data Management Office (BCO-DMO)*. https://doi.org/10.26008/1912/bco-dmo.919139.1

Lam, P. J., Lee, J.-M., Heller, M. I., Mehic, S., Xiang, Y., & Bates, N. R. (2018). Size-fractionated distributions of suspended particle concentration and major phase composition from the U.S. GEOTRACES Eastern Pacific Zonal Transect (GP16). *Marine Chemistry*, *201*, 90–107. https://doi.org/10.1016/j.marchem.2017.08.013Lam

Lam, P. J., & Marchal, O. (2015). Insights into particle cycling from thorium and particle data. *Annual Review of Marine Science*, *7*(1), 159–184. https://doi.org/10.1146/annurev-marine-010814-015623

Lane, E. S., Semeniuk, D. M., Strzepek, R. F., Cullen, J. T., & Maldonado, M. T. (2009). Effects of iron limitation on intracellular cadmium of cultured phytoplankton: Implications for surface dissolved cadmium to phosphate ratios. *Marine Chemistry*, *115*(3), 155–162. https://doi.org/10.1016/j.marchem.2009.07.008

Lane, T. W., & Morel, F. M. M. (2000). A biological function for cadmium in marine diatoms. *Proceedings of the National Academy of Sciences* (Vol. 97(9), 4627–4631). https://doi.org/10.1073/pnas.090091397

Laubach, A. (2024). Accumulation calculator (v1.0) [Software]. *Zenodo*. https://doi.org/10.5281/zenodo.14019988

Lee, J. G., & Morel, F. M. M. (1995). Replacement of zinc by cadmium in marine phytoplankton. *Marine Ecology Progress Series*, *127*, 305–309. https://doi.org/10.3354/meps127305

Lee, J.-M., Heller, M. I., & Lam, P. J. (2018). Size distribution of particulate trace elements in the U.S. GEOTRACES eastern Pacific zonal transect (GP16). *Marine Chemistry*, *201*, 108–123. https://doi.org/10.1016/j.marchem.2017.09.006

Lemaitre, N., Planquette, H., Dehairs, F., Planchon, F., Sarthou, G., Gallinari, M., et al. (2020). Particulate trace element Export in the North Atlantic (GEOTRACES GA01 transect, GEOVIDE cruise). *ACS Earth and Space Chemistry*, *4*(11), 2185–2204. https://doi.org/10.1021/acsearthspacechem.0c00045

Li, J., Babcock-Adams, L., Boiteau, R. M., McIlvin, M. R., Manck, L. E., Sieber, M., et al. (2024). Microbial iron limitation in the ocean's twilight zone. *Nature*, *633*(8031), 823–827. https://doi.org/10.1038/s41586-024-07905-z

Middag, R., van Heuven, S. M. A. C., Bruland, K. W., & de Baar, H. J. W. (2018). The relationship between cadmium and phosphate in the Atlantic Ocean unravelled. *Earth and Planetary Science Letters*, *492*, 79–88. https://doi.org/10.1016/j.epsl.2018.03.046

Morel, F. M. M., Lam, P. J., & Saito, M. A. (2020). Trace metal substitution in marine phytoplankton. *Annual Review of Earth and Planetary Sciences*, *48*(1), 491–517. https://doi.org/10.1146/annurev-earth-053018-060108

NASA Goddard Space Flight Center. (2018). Ocean ecology laboratory, Ocean biology processing group. In *Moderate-resolution imaging spectroradiometer (MODIS) aqua downwelling diffuse attenuation coefficient data*. NASA OB.DAAC. https://doi.org/10.5067/AQUA/MODIS/L3M/KD/2022

Ohnemus, D. C., Auro, M. E., Sherrell, R. M., Lagerström, M., Morton, P. L., Twining, B. S., et al. (2014). Laboratory intercomparison of marine particulate digestions including Piranha: A novel chemical method for dissolution of polyethersulfone filters. *Limnology and Oceanography: Methods*, *12*(8), 530–547. https://doi.org/10.4319/lom.2014.12.530

Ohnemus, D. C., & Lam, P. J. (2015). Cycling of lithogenic marine particles in the US GEOTRACES North Atlantic transect. *Deep-Sea Research II*, *116*, 283–302. https://doi.org/10.1016/j.dsr2.2014.11.019

Ohnemus, D. C., Rauschenberg, S., Cutter, G. A., Fitzsimmons, J. N., Sherrell, R. M., & Twining, B. S. (2017). Elevated trace metal content of prokaryotic communities associated with marine oxygen deficient zones. *Limnology & Oceanography*, *62*(1), 3–25. https://doi.org/10.1002/lno.10363

Ohnemus, D. C., Torrie, R., & Twining, B. S. (2019). Exposing the distributions and elemental associations of scavenged particulate phases in the ocean using basin-scale multi-element data sets. *Global Biogeochemical Cycles*, *33*(6), 725–748. https://doi.org/10.1029/2018GB006145

Quay, P., Cullen, J., Landing, W., & Morton, P. (2015). Processes controlling the distributions of Cd and PO4 in the ocean. *Global Biogeochemical Cycles*, *29*(6), 830–841. https://doi.org/10.1002/2014GB004998

Resing, J. A., Sedwick, P. N., German, C. R., Jenkins, W. J., Moffett, J. W., Sohst, B. M., & Tagliabue, A. (2015). Basin-scale transport of hydrothermal dissolved metals across the South Pacific Ocean. *Nature*, *523*(7559), 200–203. https://doi.org/10.1038/nature14577

Roshan, S., & DeVries, T. (2021). Global contrasts between oceanic cycling of cadmium and phosphate. *Global Biogeochemical Cycles*, *35*(6), e2021GB006952. https://doi.org/10.1029/2021GB006952

Roshan, S., & Wu, J. (2015). Cadmium regeneration within the North Atlantic. *Global Biogeochemical Cycles*, *29*(12), 2082–2094. https://doi.org/10.1002/2015GB005215

Schlitzer, R. (2023). Ocean dataview (5.6.5) [Software]. https://odv.awi.de

Seo, H., Kim, G., Kim, T., Kim, I., Ra, K., & Jeong, H. (2022). Trace elements (Fe, Mn, Co, Cu, Cd, and Ni) in the East Sea (Japan Sea): Distributions, boundary inputs, and scavenging processes. *Marine Chemistry*, *239*, 104070. https://doi.org/10.1016/j.marchem.2021.104070

Sherrell, R. M., Twining, B., & German, C. R. (2016). Trace elements in suspended particles from GO-Flo bottles [Dataset]. *Biological and Chemical Oceanography Data Management Office (BCO-DMO)*. http://lod.bco-dmo.org/id/dataset/639847

Sieber, M., Conway, T. M., de Souza, G. F., Hassler, C. S., Ellwood, M. J., & Vance, D. (2019). High-resolution Cd isotope systematics in multiple zones of the Southern Ocean from the Antarctic circumnavigation expedition. *Earth and Planetary Science Letters*, *527*, 115799. https://doi.org/10.1016/j.epsl.2019.115799

Sieber, M., Lanning, N. T., Bian, X., Yang, S.-C., Takano, S., Sohrin, Y., et al. (2023a). The importance of reversible scavenging for the marine Zn cycle evidenced by the distribution of zinc and its isotopes in the Pacific Ocean. *Journal of Geophysical Research: Oceans*, *128*(4), e2022JC019419. https://doi.org/10.1029/2022JC019419

Sieber, M., Lanning, N. T., Bunnell, Z. B., Bian, X., Yang, S.-C., Marsay, C. M., et al. (2023b). Biological, physical, and atmospheric controls on the distribution of cadmium and its isotopes in the Pacific Ocean. *Global Biogeochemical Cycles*, *37*(2), e2022GB007441. https://doi.org/10.1029/2022GB007441

Sunda, W. G., & Huntsman, S. A. (1996). Antagonisms between cadmium and zinc toxicity and manganese limitation in a coastal diatom. *Limnology & Oceanography*, *41*(3), 373–387. https://doi.org/10.4319/lo.1996.41.3.0373

Sunda, W. G., & Huntsman, S. A. (2000). Effect of Zn, Mn, and Fe on Cd accumulation in phytoplankton: Implications for oceanic Cd cycling. *Limnology & Oceanography*, *45*(7), 1501–1516. https://doi.org/10.4319/lo.2000.45.7.1501

Tian, H.-A., van Manen, M., Wille, F., Jung, J., Lee, S., Kim, T.-W., et al. (2023). The biogeochemistry of zinc and cadmium in the Amundsen Sea, coastal Antarctica. *Marine Chemistry*, *249*, 104223. https://doi.org/10.1016/j.marchem.2023.104223

Tonnard, M., Planquette, H., Bowie, A. R., van der Merwe, P., Gallinari, M., Desprez de Gésincourt, F., et al. (2020). Dissolved iron in the North Atlantic Ocean and Labrador Sea along the GEOVIDE section (GEOTRACES section GA01). *Biogeosciences*, *17*(4), 917–943. https://doi.org/10.5194/bg-17-917-2020

Tortell, P., & Price, N. (1996). Cadmium toxicity and zinc limitation in centric diatoms of the genus Thalassiosira. *Marine Ecology Progress Series*, *138*, 245–254. https://doi.org/10.3354/meps138245

Twining, B. S., & Baines, S. B. (2013). The trace metal composition of marine phytoplankton. *Annual Review of Marine Science*, *5*(1), 191–215. https://doi.org/10.1146/annurev-marine-121211-172322

Twining, B. S., Rauschenberg, S., Morton, P. L., Ohnemus, D. C., & Lam, P. J. (2015). Comparison of particulate trace element concentrations in the North Atlantic Ocean as determined with discrete bottle sampling and in situ pumping. *Deep Sea Research Part II: Topical Studies in Oceanography*, *116*, 273–282. https://doi.org/10.1016/j.dsr2.2014.11.005

Wong, K. H., Obata, H., Ikhsani, I. Y., & Muhammad, R. (2021). Controls on the distributions of dissolved Cd, Cu, Zn, and Cu-binding organic ligands in the East China Sea. *Journal of Geophysical Research: Oceans*, *126*(66). https://doi.org/10.1029/2020jc016997

Wu, J. (2017). Dissolved Fe, Mn, Cd, Cu and Zn concentrations from bottle samples during the R/V Thomas G. Thompson TN303 GEOTRACES EPZT cruise in the Eastern Tropical Pacific from November to December 2013 (U.S. GEOTRACES EPZT) [Dataset]. *Biological and Chemical Oceanography Data Management Office (BCO-DMO)*. http://lod.bco-dmo.org/id/dataset/671150

Xiang, Y., & Lam, P. J. (2020). Size-fractionated compositions of marine suspended particles in the Western Arctic Ocean: Lateral and vertical Sources. *Journal of Geophysical Research: Oceans*, *125*(8), e2020JC016144. https://doi.org/10.1029/2020JC016144

Xiang, Y., Lam, P. J., Burd, A. B., & Hayes, C. T. (2022). Estimating mass flux from size-fractionated filtered particles: Insights into controls on sinking velocities and mass fluxes in recent U.S. GEOTRACES cruises. *Global Biogeochemical Cycles*, *36*(44). https://doi.org/10.1029/2021gb007292

Xie, R. C., Galer, S. J. G., Abouchami, W., Rijkenberg, M. J. A., De Jong, J., de Baar, H. J. W., & Andreae, M. O. (2015). The cadmium–phosphate relationship in the Western South Atlantic — The importance of mode and intermediate waters on the global systematics. *Marine Chemistry*, *177*, 110–123. https://doi.org/10.1016/j.marchem.2015.06.011

Xu, Y., Tang, D., Shaked, Y., & Morel, F. M. M. (2007). Zinc, cadmium, and cobalt interreplacement and relative use efficiencies in the coccolithophore Emiliania huxleyi. *Limnology & Oceanography*, *52*(5), 2294–2305. https://doi.org/10.4319/lo.2007.52.5.2294

Yang, Z., Sohrin, H., Sohrin, Y., & Ho, T. Y. (2018). Cadmium cycling in the water column of the Kuroshio-Oyashio extension region: Insights from dissolved and particulate isotopic composition. *Geochimica et Cosmochimica Acta*, *233*, 66–80. https://doi.org/10.1016/j.gca.2018.05.001

Zhang, R., Jensen, L. T., Fitzsimmons, J. N., Sherrell, R. M., & John, S. (2019). Dissolved cadmium and cadmium stable isotopes in the western Arctic Ocean. *Geochimica et Cosmochimica Acta*, *258*, 258–273. https://doi.org/10.1016/j.gca.2019.05.028